ACS APPLIED MATERIALS & INTERFACES

Research Article

www.acsami.org

Reduction-Responsive Core–Shell–Corona Micelles Based on Triblock Copolymers: Novel Synthetic Strategy, Characterization, and Application As a Tumor Microenvironment-Responsive Drug Delivery System

Xubo Zhao and Peng Liu*

State Key Laboratory of Applied Organic Chemistry and Key Laboratory of Nonferrous Metal Chemistry and Resources Utilization of Gansu Province, College of Chemistry and Chemical Engineering, Lanzhou University, Lanzhou 730000, China

Supporting Information

ABSTRACT: A facile and effective approach was established for fabricating core–shell–corona micelles by self-assembly of poly(ethylene glycol)-*b*-poly(acrylic acid-*co*-*tert*-butyl acrylate)-poly(ε-caprolactone) (PEG_{43}-*b*-P(AA_{30}-*co*-*t*BA_{18})-*b*-PCL_{53}) triblock copolymer, synthesized via a combination of ring-opening polymerization (ROP), atom transfer radical polymerization (ATRP), click chemistry, and hydrolyzation. The prenanovehicles with three different hydrolysis degrees from PEG_{43}-*b*-P*t*BA_{48}-*b*-PCL_{53} were developed to evaluate the drug loading capacity (DLC) and drug encapsulation efficiency (DEE). After cross-linking with a disulfide bond to regulate the drug release kinetics, the spherical core–shell–corona micelles with average diameter of 52 ± 4 nm were obtained in aqueous solution. The reduction-responsive cross-linked micelles showed a slow sustained release in normal physiological conditions and a rapid release upon exposure to simulated tumor intracellular conditions. In addition, the cytotoxic analysis and HepG2 cell growth inhibition assays demonstrated their remarkable biocompatibility and similar excellent anticancer activity as the free doxorubicin (DOX), which has also been revealed by the confocal laser scanning microscope (CLSM) analysis. So the reduction-sensitive core–shell–corona micelles are expected to be promising tumor microenvironment-responsive nanovehicles for hydrophobic drugs by glutathione (GSH) triggering.

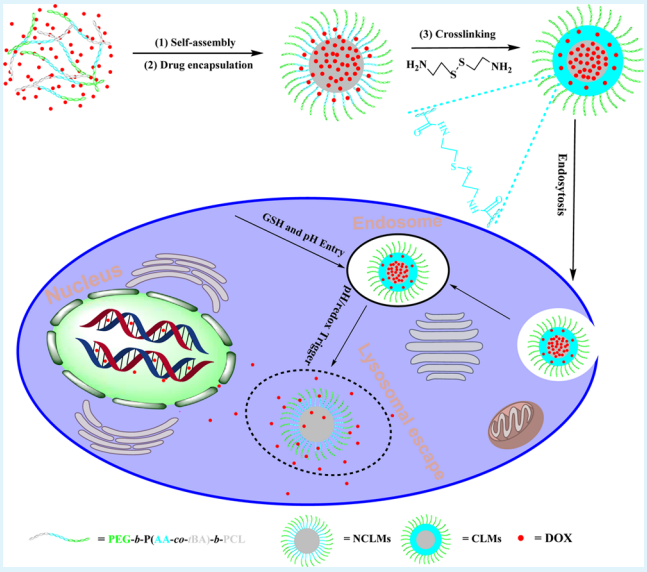

KEYWORDS: *triblock copolymer, core–shell–corona micelle, design, tumor microenvironment-responsive, drug delivery system*

INTRODUCTION

In the last decades, polymeric micelles have received intense attraction as nanovehicles for cancer diagnosis and therapy, due to their distinct advantages including passive targeting ability to tumor tissues through the enhanced permeability and retention (EPR) effect, encapsulating capacity to drugs, improvement of drug solubility, and high tunability of stimuli-responsive release.[1] A unique architecture is provided as drug delivery vehicles by the self-assembled polymeric micelles from the amphiphilic block copolymers, in which their hydrophobic cores undertake the task of drug loading and regulate the release of the hydrophobic drugs (such as doxorubicin (DOX)), while their hydrophilic shells endow their stability in bodily fluids.[2]

However, several problems associated with the practical application result in a despondent clinical outcome.[3] Consequently, the embarrassing situation has facilitated the ever increasing attention in amphiphilic block copolymers for drug delivery systems (DDSs).[4] Amphiphilic block copolymers containing both hydrophilic and hydrophobic blocks can be self-assembled into micelles as vehicles for hydrophobic drugs. However, in further applications for anticancer drug delivery, the performance of the self-assembled micelles might be limited by suffering from low structural stability and tending to be disrupted upon large dilution. The dissociation of self-assembly at low concentrations (below its critical micelle concentration (CMC)) in blood circulation indeed accelerates the premature drug release at normal tissues or organs; thus only a low extent of vehicle dosage could reach the target disease sites,[5] and the premature drug release usually leads to serious side effects. To

Received: August 17, 2014
Accepted: November 14, 2014
Published: November 14, 2014

Scheme 1. Schematic Illustration of the Composition, Self-Assembly, and Drug Release of the Core−Shell−Corona DDS by GSH and pH Triggers

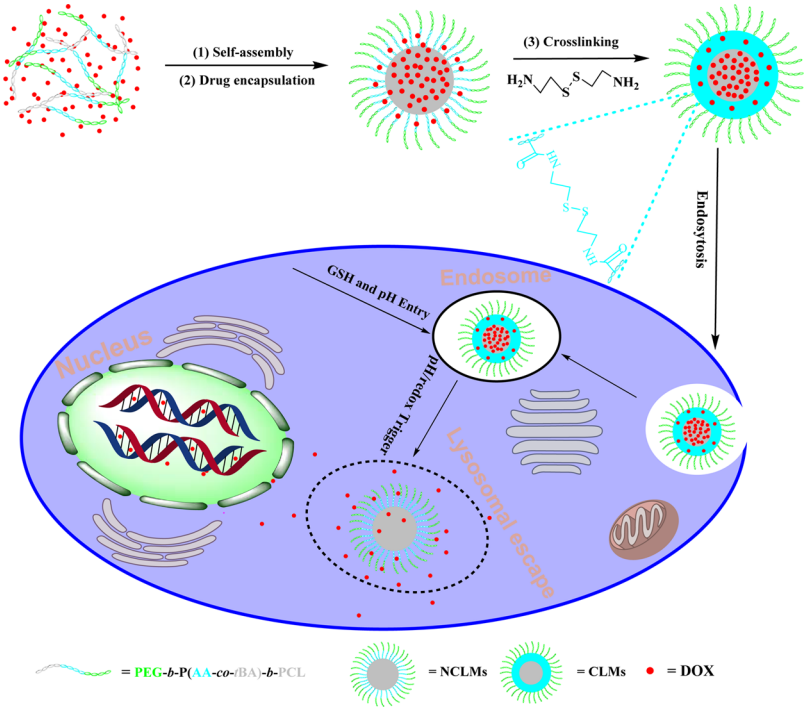

resolve the stability issue, conventional chemical cross-linking of micelles has been used as a powerful approach to hold the self-assembled architecture.[6] However, the cross-linked shell might limit the intracellular drug release. To satisfy the requirement, the degradable linkages have been utilized as a promising approach for shell cross-linking. The intracellular microenvironments of the tumor tissues are drastically different from the normal tissues, such as acidic pH inside endosomes and lysosomes (pH 4.5−6.5),[7] and reductive conditions because of a high level of glutathione (GSH) or cysteine in the cytoplasm and endolysosomes.[8] So the reduction-sensitive micelles have been extensively investigated to design the intracellular delivery system with a disulfide bond as a reductively cleavable linkage in response to GSH in the cytoplasm and endolysosomes recently. Biodegradable Y-shaped amphiphilic block copolymer mPEG-*b*-PLG-*b*-$(PLA)_2$ was synthesized, and the inner shells of their micelles were cross-linked with cystamine. The cross-linked micelles showed reduction-responsive controlled release of DOX and much higher *in vitro* stability than the non-cross-linked micelles.[9]

Zhong reported that the cross-linked poly(ethylene oxide)-*b*-poly(acrylic acid)-*b*-poly(*N*-isopropylacrylamide) with cystamine as the cross-linker showed remarkable stability against dilution but rapidly disintegrated upon reductive media mimicking tumor intracellular microenvironments.[10]

In most cases, the micelles have been self-assembled with the amphiphilic block copolymers, such as diblock copolymer, triblock copolymer, and multiblock copolymer, etc. The category of the diblock copolymer of poly(ε-caprolactone)-*b*-poly(ethylene glycol) (PCL-*b*-PEG) has been utilized as biodegradable and biocompatible DDSs.[11] Lang's group prepared an amphiphilic block copolymer based on PCL-*b*-PEG for micellar DDS with improved solubilization and DOX-delivery performance.[12] Compared with diblock copolymers, the polymeric micelles from the triblock copolymers have unique structure and versatile characteristics. Liu and coauthors reported the core−shell−corona micelles self-assembled by the thermoresponsive PEG-*b*-PNIPAM-*b*-PCL.[13] Dong's group reported the polycation-detachable nanoparticles based on mPEG-PCL-*g*-SS-PDMAEMA for siRNA delivery.[14] In addition, Gan and co-workers reported a thermosensitive core−shell nanoparticle by self-assembling a triblock copolymer (PCL-*b*-PEO-*b*-PNIPAm) as the DDS for controlled release.[15] Kissel et al. synthesized an amphiphilic triblock copolymer (PEG-PCL-PEI) for the codelivery of nucleic acids, drugs, and/or dyes.[16]

Du and co-workers reported the block copolymer of PEO-*b*-P(AA-*stat*-*t*BA) via ATRP and partial hydrolysis for drug delivery.[17] On the basis of the research, they reported another interesting study of a triblock copolymer vesicle (PEO_{113}-*b*-PCL_{132}-*b*-PAA_{15}) with an asymmetrical structure for rapid endocytosis rate and much faster endosomal escape ability for anticancer application.[18] In their works, *t*BA had been used to design the block via ATRP and then hydrolyzed into a PAA block or partially hydrolyzed into a P(AA-*stat*-*t*BA) block. This approach could effectively regulate the hydrophilic and hydrophobic characteristics of the copolymer. What's more, the produced carboxyl groups are expected to be used for the cross-linking of the core−shell−corona self-assembled micelles.

In this work, a poly(ethylene glycol)-*b*-poly(acrylic acid-*co*-*tert*-butyl acrylate)-poly(ε-caprolactone) (PEG_{43}-*b*-P(AA_{30}-*co*-tBA_{18})-*b*-PCL_{53}) triblock copolymer was designed by the combination strategy of ring-opening polymerization (ROP), atom transfer radical polymerization (ATRP), click chemistry, and hydrolyzation. The core−shell−corona reducible disulfide-bond-cross-linked micelles were assembled as a biocompatible, stable, and smart nanocarrier and preferentially released the encapsulated DOX responding to GSH (Scheme 1). The hydrophobic segments gradually collapse on the PCL core to encapsulate DOX; the disulfide bond cross-linked PAA shell

dx.doi.org/10.1021/am505531e | *ACS Appl. Mater. Interfaces* 2015, 7, 166−174

brings down the DOX prematurely during blood circulation and is more rapidly released in target disease sites; and the PEG corona endows the stealthy features during blood circulation.

EXPERIMENTAL SECTION

Materials and Reagents. Poly(ethylene glycol) monomethyl ether (PEG_{43}) was obtained from Beijing Kaizheng Bioeng. Development Co. Ltd. ε-Caprolactone (CL) was provided by Aladdin Ind. Co., dried over CaH_2 for 48 h at room temperature, and distilled under reduced pressure before use. Doxorubicin hydrochloride (DOX·HCl) was purchased from Beijing Huafeng United Technology Co. Ltd.

Stannous octanoate ($Sn(Oct)_2$) (Sinopharm Co. Ltd.) was purified as reported previously.[19] 1-Ethyl-3-(3-dimethyl aminopropyl) carbodiimide hydrochloride (EDC·HCl) was provided by Fluorochem. *N*-Hydroxylsuccinimide (NHS) was purchased from Aladdin Chem. Co. Ltd. Tetrahydrofuran (THF) was refluxing over sodium (Na) and distilled in N_2 atmosphere just before use. Triethylamine (TEA) and toluene were dried over CaH_2 for 48 h at room temperature and distilled under reduced pressure before use. *Tert*-butyl acrylate (*t*BA) was obtained from J & K Chem. Ltd. Copper(I) bromide (Cu(I)Br, 99.5%) from Sinopharm Co. Ltd. was purified extensively in a solution of acetic acid by magnetic stirring for 24 h in the dark, washing extensively with ethyl alcohol, ethyl ether, and acetone, and drying under vacuum. *N,N,N″,N″*-Pentamethyl diethylenetriamine (PMDETA, 99%), dimethylformamide (DMF), 2-bromoisobutyryl bromide (BIBB, 98%), and sodium azide were used directly from Aladdin Ind. Co. All other reagents were analytic reagent grade from Tianjin Chem. Co. Ltd. and used without further purification. Double distilled water was used throughout.

PEG_{43}-Br. After 10 g of PEG_{43} was dissolved in 150 mL of toluene, approximately 40 mL of toluene with traces of water was removed from the mixture by azeotropic distillation at reduced pressure. Then 2.5 mL of TEA was added into the solution at 0 °C. Subsequently, 2.0 mL of BIBB was added dropwise via a constant pressure funnel in 40 min with magnetic stirring, and the reaction was performed with moderate stirring overnight at room temperature. After most toluene was removed at reduced pressure, the product was precipitated in excess cold ether. The precipitate was dried under vacuum, dissolved in 20 mL of pH 8−9 $NaHCO_3$ aqueous solution, and extracted with CH_2Cl_2. Finally, the organic phase was gathered and dried over $MgSO_4$. Finally CH_2Cl_2 was removed completely at reduced pressure to obtain the resultant macroinitiator (PEG_{43}-Br).[20]

PEG_{43}-*b*-P*t*BA_{48}. PEG_{43}-*b*-P*t*BA_{48} was synthesized via the ATRP of *t*BA with the macroinitiator PEG_{43}-Br. An amount of 1.834 g (0.885 mmol) of PEG_{43}-Br was dissolved in 6 mL of anhydrous THF. After the mixture was gassed and degassed under N_2, 0.153 g (0.885 mmol) of PMDETA and 6.756 g (53.71 mmol) of *t*BA were charged under degassing by freeze−pump−thaw in a N_2 atmosphere, followed by adding 0.127 g (0.885 mmol) of CuBr and then degassing. Subsequently, ATRP was carried out at 45 °C for 8 h with the conversion of *t*BA of 80% from the information on ^1H NMR analysis. The copper catalyst in the resultant solution was removed with an alumina column, after dilution with THF. The block copolymer PEG_{43}-*b*-P*t*BA_{48} was precipitated in cold ether and dried in vacuum overnight at room temperature.

PEG_{43}-*b*-P*t*BA_{48}-*b*-PCL_{53}. The PEG_{43}-*b*-P*t*BA_{48}-N_3 was synthesized by a similar procedure,[13] with conversion of 61.5% for 0.032 g (0.493 mmol) of NaN_3 and 2.0 g (0.247 mmol) of PEG_{43}-*b*-P*t*BA_{48} in 20 mL of DMF. The propargyl-terminated PCL (M_n = 6200, M_w/M_n = 1.12) was synthesized by a similar procedure,[13,21] with ε-CL conversion of 48.2% from the ^1H NMR analysis.

The click reaction of the PEG_{43}-*b*-P*t*BA_{48}-N_3 and propargyl-terminated PCL was carried out as follows: 0.0143 g (0.10 mmol) of Cu(I)Br, 0.605 g (0.10 mmol) of propargyl-terminated PCL_{53}, and 0.977 g (0.12 mmol) of PEG_{43}-*b*-P*t*BA_{48}-N_3 were added into 10 mL of THF with stirring. After the mixture was gassed and degassed under N_2, 0.0173 g (0.10 mmol) of PMDETA was introduced via a degassed syringe. The click reaction was then performed with stirring for 24 h at room temperature. After that, the copper catalyst within resultant solution was removed through an alumina column. The mixture was dialyzed against THF/water (v/v, 2/1) with a dialysis membrane (MWCO of 10 000) for 2 days, and subsequently the copolymer was dried under vacuum overnight at room temperature. Finally, 1.294 g of PEG_{43}-*b*-P*t*BA_{48}-*b*-PCL_{53} was obtained.

Hydrolysis of PEG_{43}-*b*-P*t*BA_{48}-*b*-PCL_{53}. The triblock copolymer was dissolved in a THF/water mixture (v/v, 7/1), and a 2-fold molar excess of NaOH (with respect to the *t*BA units) was added and stirred at room temperature for 24 h. Most of the THF was removed at reduced pressure by a rotary evaporator. The hydrolytic copolymers of PEG_{43}-*b*-P(AA_{30}-*co*-*t*BA_{18})-*b*-PCL_{53} were obtained by lyophilization for 6 h.

The PEG_{43}-*b*-P(AA_{16}-*co*-*t*BA_{32})-*b*-PCL_{53} was obtained in the presence of half-fold molar NaOH by a similar procedure, to demonstrate the effect of the different hydrolysis degrees of the P*t*BA segment on the drug loading capacity.

Micellization and DOX Loading. The DOX-loaded micelles of PEG_{43}-*b*-P(AA_{30}-*co*-*t*BA_{18})-*b*-PCL_{53}, PEG_{43}-*b*-P*t*BA_{48}-*b*-PCL_{53}, and PEG_{43}-*b*-P(AA_{16}-*co*-*t*BA_{32})-*b*-PCL_{53} were prepared with a procedure similar to that reported previously,[9] with 10 mg of DOX and 50 mg of copolymer in 10 mL THF/50 mL PBS solution (10 mM, pH 7.4).

Cross-Linking of Micelles. Cystamine was utilized to covalently cross-link the carboxyl groups of the PAA moieties for preparing the DOX-loaded shell-cross-linked micelles with reduction-response (DOX-loaded PEG_{43}-*b*-P(AA_{30}-*co*-*t*BA_{18})-*b*-PCL_{53} CLMs). In a typical procedure, 100 mg of DOX-loaded PEG_{43}-*b*-P(AA_{30}-*co*-*t*BA_{18})-*b*-PCL_{53} micelles was dispersed into 50 mL of PBS solution. Amounts of 2.0 equiv of NHS (to carboxyl groups), 2.0 equiv of EDC·HCl, and 0.5 equiv of cystamine dihydrochloride were introduced into the above mixture after its pH value was regulated to 5.5 by diluted HCl. Subsequently, the suspension was performed under magnetic stirring at room temperature for 24 h. Finally, the excess DOX, NHS, and cystamine were removed by dialysis for 24 h.

Cell Toxicity Assays. MTT (3-(4,5-dimethylthiazol-2-yl)-2,5-diphenyltetrazolium bromide) assay was performed to evaluate the biocompatibility of the cross-linked PEG_{43}-*b*-P(AA_{30}-*co*-*t*BA_{18})-*b*-PCL_{53} micelles with HepG2 cells, and its inhibition growth ability was also evaluated with DOX as the model drug. After the cells were seeded in 96-well plates for 24 h, the cross-linked PEG_{43}-*b*-P(AA_{30}-*co*-*t*BA_{18})-*b*-PCL_{53} micelles with or without being treated with 10 mM GSH for 48 h, DOX-loaded cross-linked PEG_{43}-*b*-P(AA_{30}-*co*-*t*BA_{18})-*b*-PCL_{53} micelles, or free DOX with different concentrations were added and incubated for 24 h. Then the cells were washed with PBS for the cell viability by the MTT assay: 100 μL of PBS solution containing 1.0 mg/mL of MTT was added into each well and incubated for 4 h, following a draw of the medium. Then the cell-bound dye was dissolved with 100 μL of DMSO, and the absorbance was read with a microplate reader at 490 nm.

Controlled Release. The dispersion of the DOX-loaded cross-linked PEG_{43}-*b*-P(AA_{30}-*co*-*t*BA_{18})-*b*-PCL_{53} micelles (10 mg in 10 mL) in PBS (pH 7.4 no GSH, pH 7.4 and 10 μM GSH, pH 5.0 no GSH, or pH 5.0 and 10 mM GSH) was transferred into dialysis tubes (MWCO of 10 000) and immersed in 120 mL of PBS at 37 °C, respectively. A 5.0 mL aliquot solution was taken out to detect the drug concentration with a UV spectrophotometer at certain time intervals, and 5.0 mL of fresh relevant PBS was complemented after each sampling. The cumulative release was expressed as the total percentage of drug released over time, as follows

$$M_i = C_i \times 120\ \text{mL} + \Sigma_{j=1}^{j=i-1} C_j \times 5\ \text{mL}$$

$$\text{Cumulative release (\%)} = (M_i/M_A) \times 100\%$$

where M_i is the total cumulative drug mass released from the nanocarriers of measurement i; C_i (mg/mL) is the drug concentration of sample i; $\sum_{j=1}^{j=i-1} C_j \times 5$ mL is the total drug mass in previously extracted samples; and M_A is the total drug mass loaded in the nanocarriers.

For comparison, the DOX release of the PEG_{43}-*b*-P(AA_{30}-*co*-*t*BA_{18})-*b*-PCL_{53} micelles (NCMs) was investigated in PBS (pH 7.4 no GSH, or pH 5.0 no GSH) under the same conditions.

The Higuchi and Korsmeyer–Peppas release equations were carried out to analyze release data, as below

$$M_t = k \cdot t^{1/2}$$

where M_t is the drug released at time t, and k is the rate constant. Once a plot of M_t vs $t^{1/2}$ is linear with a slope ≥1, it is considered to follow the Higuchi drug release kinetics[22]

$$M_t/M_\infty = k \cdot t^n \qquad M_t/M_\infty < 0.6$$

where M_t/M_∞ is the drug release fraction at time t; k is a constant; and n is the release exponent.[23]

CLSM Analysis. The confocal laser scanning microscope (CLSM) technique was used to investigate the cellular uptake of the DOX-loaded CLMs for HepG2 cells, as reported previously.[24]

Analysis and Characterizations. ^{1}H NMR spectra were recorded with an Advance 400 MHz spectrometer at room temperature, with $CDCl_3$ as solvent.

The Fourier transform infrared (FT-IR) spectra were recorded with a Bruker IFS 66 v/s infrared spectrometer in 400–4000 cm^{-1} with a resolution of 4 cm^{-1}.

The number-average molecular weight (M_n) and polydispersity (PDI) of the copolymers were measured by gel permeation chromatography (GPC) in THF at 35 °C.

The critical micelle concentrations (CMCs) of the copolymers were determined by measuring the fluorescence intensity with a Hitachi F-4500 fluorescence spectrophotometer in acetone solution with pyrene as a probe.

The micellar morphologies were analyzed with a JEM-1200 EX/S transmission electron microscope (TEM). The aqueous dispersions of the samples were deposited on a copper grid covered with a perforated carbon film and stained with 2% phosphotungstic acid, dried at room temperature in vacuum.

The dynamic light scattering (DLS) measurements were carried out with a Light Scattering System BI-200SM device equipped with a BI-200SM Goniometer, a BI-9000AT Correlator, a temperature controller, and a coherent INOVA 70C Argonion laser at 20 °C. DLS measurements were performed using a 135 mW intense laser excitation at 514.5 nm at a detection angle of 90° using the dispersions directly at 25 °C.

The release performance of the PEG_{43}-*b*-P(AA_{30}-*co*-*t*BA_{18})-*b*-PCL_{53} (NCMs) and the cross-linked PEG_{43}-*b*-P(AA_{30}-*co*-*t*BA_{18})-*b*-PCL_{53} (CLMs) micelles was assessed with a PerkinElmer Lambda 35 UV–vis spectrometer at room temperature.

RESULTS AND DISCUSSION

Synthesis and Characterization of Block Copolymers. In the present work, novel triblock copolymers PEG_{43}-*b*-(PAA_n-*co*-*t*BA_{48-n})-*b*-PCL_{53} with different hydrolysis degrees were synthesized through a combination of ROP, ATRP, click reaction, and hydrolysis reaction (Scheme 2). In the ^{1}H NMR spectrum of the CH_3O–PEG_{43}–OH (Figure 1), the characteristic signal of the inner methylene protons adjacent to the oxygen moieties (b, O–CH_2) at δ =3.65 ppm is shown in curve A, and the chemical shift at δ = 3.38 ppm is assigned to the terminal methyl protons (a, O–CH_3). The characteristic signal of the methyl protons (c, C(Br)–CH_3) at δ= 1.94 ppm reveals the presence of the 2-bromoisobutyryl groups (Figure 1 (curve B)). It is clear that CH_3O–PEG_{43}–OH was completely transformed into the PEG_{43}-Br, from the peak areas of c and a. Besides the characteristic signals of PEG, the chemical shift of P*t*BA at δ = 1.44 ppm (d) representing the methyl protons of the *t*-butyl groups appeared (Figure 1 (curve C)), revealing the PEG_{43}-*b*-P*t*BA_{48} diblock copolymer has been successfully obtained. In addtion, the average DP_n of the PEG_{43}-*b*-P*t*BA_{48} diblock copolymer is concluded based on the peak area ratios between d and b.

Scheme 2. Synthesis Procedure of the Triblock Copolymer PEG_{43}-*b*-(PAA_n-*co*-*t*BA_{48-n})-*b*-PCL_{53}

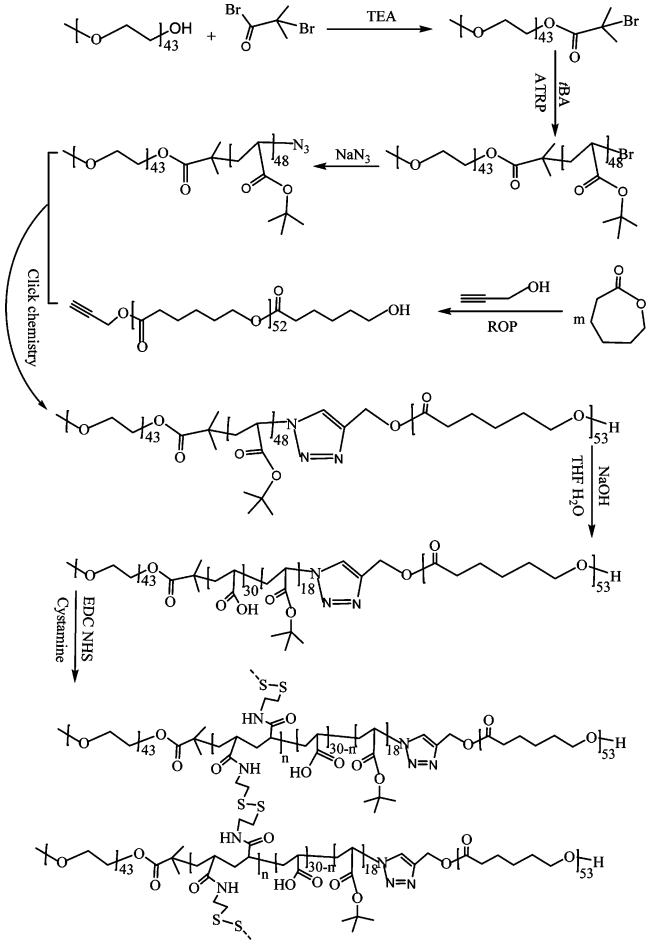

Compared with the CH_3O–PEG_{43}–OH, the new characteristic absorbance at 1735 cm^{-1} of carbonyl stretching vibration in ester groups appeared in the FT-IR spectrum of the PEG_{43}-Br (Figure S1, Supporting Information). The finding demonstrates the conversion from CH_3O–PEG_{43}–OH to PEG_{43}-Br. Meanwhile, the PEG_{43}-*b*-P*t*BA_{48} diblock copolymer is prepared via the ATRP of *t*BA with PEG_{43}-Br as the macroinitiator. Moreover, the FT-IR spectrum also is carried out to confirm the preparation of the PEG_{43}-*b*-P*t*BA_{48} diblock copolymer. Compared to PEG_{43}-Br, the discovery of characteristic absorbance at 1394 cm^{-1} is associated with *t*-butyl groups.

According to GPC results (Figure S2, Supporting Information), the polydispersity (M_w/M_n) and the number-average molecular weight (M_n) of the PEG_{43}-*b*-P*t*BA_{48} are 1.21 and 8600, respectively. The ATRP reaction was terminated at relatively low conversion to ensure a high degree of bromine end functionality.[25] Subsequently PEG_{43}-*b*-P*t*BA_{48}-N_3 was synthesized from the terminal bromine of the PEG_{43}-*b*-P*t*BA_{48} by the simple nucleophilic substitution reaction in DMF solution with excess NaN_3. The appearance of a new absorbance around 2100 cm^{-1} of the terminal azido group reveals that the terminal bromine of PEG_{43}-*b*-P*t*BA_{48} has been transformed into an azide group (Figure S1, Supporting Information (curve d)).[26]

dx.doi.org/10.1021/am505531e | ACS Appl. Mater. Interfaces 2015, 7, 166–174

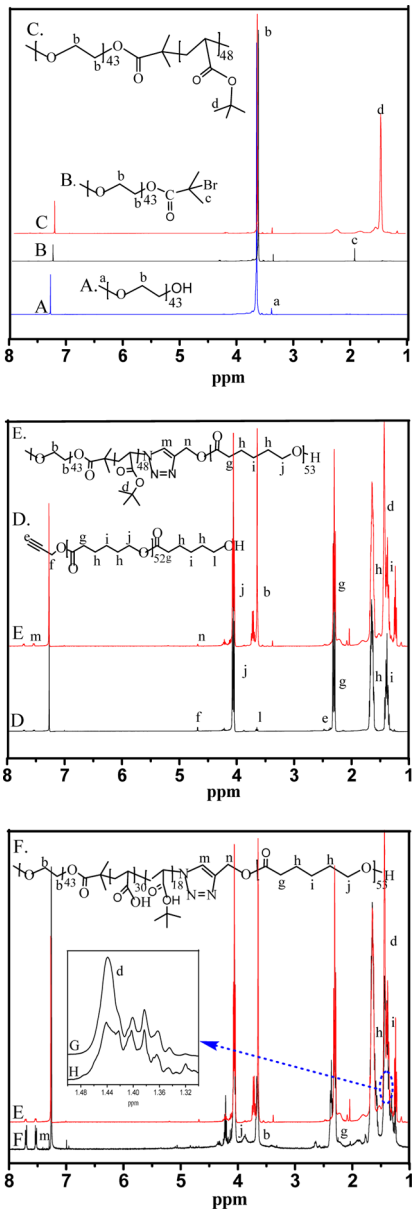

Figure 1. ^{1}H NMR spectra of (A) PEG_{43}, (B) PEG_{43}-Br, (C) PEG_{43}-*b*-P*t*BA_{48}, (D) propargyl-terminated PCL_{53}, (E) PEG_{43}-*b*-P*t*BA_{48}-*b*-PCL_{53}, and (F) PEG_{43}-*b*-P(AA_{30}-*co*-*t*BA_{18})-*b*-PCL_{53}.

The preparation of PCL was performed via ROP of ε-CL using propargyl alcohol as initiator in toluene at 120 °C, revealed by the ^{1}H NMR information (Figure 1 (curve D)). The chemical shift at δ = 4.69 ppm (f) is assigned to the characteristic signal of methylene protons of the propargyl group, with the resonance of the alkynyl proton (e) overlapped with the PCL_{53} methylene protons at 2.31 ppm (g). The resonance at δ =3.65 ppm (l) is assigned to the methylene proton of PCL_{53} adjacent to the hydroxyl end group. So the DP_n of the liner polymer PCL could be assessed from the area ratio of signals at 4.06 ppm (j) of the repeating units and 3.65 ppm (l). Meanwhile, the PCL showed a low polydispersity index from the GPC results (Figure S2, Supporting Information).

The well-defined PEG_{43}-*b*-P*t*BA_{48}-*b*-PCL_{53} copolymer was prepared via the classical click reaction between the propargyl-terminated PCL_{53} and azide end groups of the PEG_{43}-*b*-P*t*BA_{48} in the presence of Cu(I)Br/PMDETA in anhydrous THF at 25 °C, in which excess propargyl-terminated PCL_{53} was utilized to make the click chemistry complete, and the unreacted propargyl-terminated PCL_{53} was removed using dialysis after the click reaction. In Figure 1 (curve F), the resonance of whole the protons of the PEG_{43}-*b*-P*t*BA_{48} and PCL_{53} segments can be assigned, but even more crucial, the new chemical shifts at δ = 4.72 ppm (n) and δ = 7.66 ppm (m) are assigned to methylene protons in PCL adjacent to the 1,2,3-trizole rings, revealing the successful cycloaddition. Compared with PEG_{43}-*b*-P*t*BA_{48}-N_3, the peak at 2100 cm^{-1} of $-N_3$ disappeared completely, while the peak at 1241 cm^{-1} associated with the methylene of PCL_{53} segments appeared (Figure S1 (curve e), Supporting Information), also indicating the successful click chemistry. In addition, compared with the molecular weight of the PEG_{43}-*b*-P*t*BA_{48} and PCL_{53}, the GPC curve of the PEG_{43}-*b*-P*t*BA_{48}-*b*-PCL_{53} apparently shifted toward high molecular weight (Figure S2, Supporting Information). The result demonstrates that cycloaddition reaction between the PEG_{43}-*b*-P*t*BA_{48}-N_3 and the propargyl-terminated PCL_{53} was realized. Furthermore, the signal area ratio of g and b in the ^{1}H NMR spectrum (Figure 1 (curve E)) is consistent with the theoretical value, demonstrating the unique structure of the PEG_{43}-*b*-P*t*BA_{48}-*b*-PCL_{53} triblock copolymer.

Finally, the controlled hydrolysis of the P*t*BA block was performed in its THF/water (v/v, 7/1) solution. Three different amounts of NaOH were utilized to obtain the P(AA-*co*-*t*BA) segments to achieve the optimized drug loading capacity (DLC) and encapsulation efficiency (DEE) (Table 1). The hydrolysis degree of P*t*BA could be assessed via the signal area ratio of δ = 3.65 ppm (b) and δ = 1.44 ppm (d). Compared with the PEG_{43}-*b*-P*t*BA_{48}-*b*-PCL_{53}, the hydrolysis degrees of 33.3% and 62.5% for the P*t*BA segments were obtained in the presence of 0.5 and 2.0 equiv of NaOH, respectively (Figure S3, Supporting Information). The hydrolysis of the P*t*BA moieties is not complete in basic media due to adjacent group effects of the polymer.

Micellization. The triblock copolymer is composed of hydrophobic (*t*BA units and PCL block) and hydrophilic (AA units and PEG block) segments and thus is expected to form unique micelles. The micelles were prepared via solvent dialysis, and their size and morphology were tracked by DLS technology

Table 1. Some Important Parameters

polymers	DP_{tBA}[a]	DP_{AA}[a]	DP_{CL}[a]	CMC[b]	Size[c]	DLC[d]	DEE[d]
PEG_{43}-*b*-P*t*BA_{48}-*b*-PCL_{53}	48	0	53	0.79	89 ± 39	21.3%	42.6%
PEG_{43}-*b*-P(AA_{16}-*co*-*t*BA_{32})-*b*-PCL_{53}	32	16	53	1.91	58 ± 18	26.4%	52.8%
PEG_{43}-*b*-P(AA_{30}-*co*-*t*BA_{18})-*b*-PCL_{53}	18	30	53	2.82	55 ± 5	31.1%	62.2%
CLMs	18	30	53	-	52 ± 4	28.5%	57.0%

[a]The DP was determined by ^{1}H NMR. [b]The CMC (mg/L) was determined by a fluorescence spectrophotometer. [c]The diameter of micelles was determined by TEM. [d]The DLC and DEE (%) were assessed with a UV−vis spectrometer.

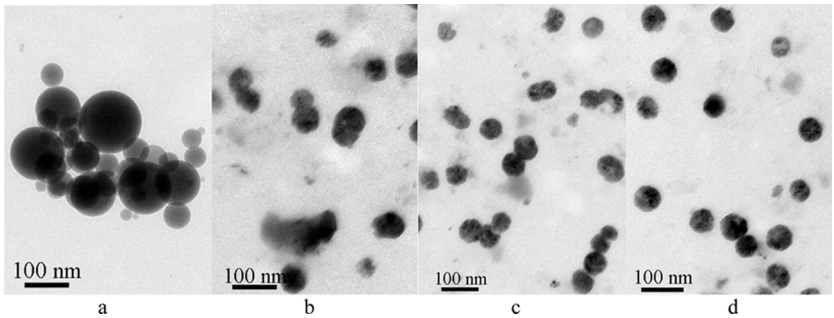

Figure 2. TEM images of the micelles of the copolymers: (a) PEG_{43}-*b*-$PtBA_{48}$-*b*-PCL_{53}, (b) PEG_{43}-*b*-P(AA_{16}-*co*-tBA_{32})-*b*-PCL_{53}, (c) PEG_{43}-*b*-P(AA_{30}-*co*-tBA_{18})-*b*-PCL_{53}, and (d) shell cross-linked PEG_{43}-*b*-P(AA_{30}-*co*-tBA_{18})-*b*-PCL_{53}.

in aqueous solution at pH 7.4 and TEM, respectively. The effect of the hydrophobic segment length on the micelles was also investigated with different hydrolysis degrees. The triblock copolymer PEG_{43}-*b*-$PtBA_{48}$-*b*-PCL_{53} could only form spherical particles ranging from 40 to 120 nm (Figure 2a), due to its long hydrophobic blocks. Increasing the hydrophilic moieties from the PEG_{43}-*b*-PAA_{16} to the PEG_{43}-*b*-PAA_{30}, the hydrophobic segments were dramatically reduced. The change results in the micelles of the PEG_{43}-*b*-P(AA_{30}-*co*-tBA_{18})-*b*-PCL_{53} with regular morphology and narrow size distribution (Figure 2b and c). So the average diameters of the micelles could be adjusted by varying the ratio of the PtBA-*b*-PCL to the PEG-*b*-PAA blocks.

For the micelles, the critical micelle concentration (CMC) plays an extremely important role in the biomedical applications.[27] The micelle with a lower CMC always possesses a better dilution stability. The CMC increased for both the PEG_{43}-*b*-P(AA_{16}-*co*-tBA_{32})-*b*-PCL_{53} and the PEG_{43}-*b*-P(AA_{30}-*co*-tBA_{16})-*b*-PCL_{53} copolymers, with decreasing hydrophobic blocks (Table 1), as reported previously.[28]

Cross-Linking of Micelles. To solve the stability issue and obtain the desired core−shell−corona polymeric micelles, cystamine was utilized as a cross-linker to react with the carboxyl groups in the triblock copolymers via the carbodiimide coupling in the presence of EDC/NHS. Compared with the non-cross-linking micelles (NCMs), the cross-linked PEG_{43}-*b*-P(AA_{30}-*co*-tBA_{18})-*b*-PCL_{53} micelles (CLMs) were endowed perfect morphology and narrow size distribution by tracking TEM (Figure 2d) and DLS technologies (Figure S4 (curves B and C), Supporting Information). The hydrodynamic diameter of the CLMs (Figure S4 (curve C), Supporting Information) became smaller, compared with the NCMs (Figure S4 (curve B), Supporting Information).

To demonstrate the successful cross-linking, the hydrodynamic diameter of the CLMs and the NCMs was also determined by DLS in a water/THF (v/v, 1:6) mixture solvent, after the micelle suspension was shaken at 37 °C for 6 h in order to achieve dispersion. Only the small matters (polymer) were detected for the NCMs upon adding THF (Figure S4 (curves C, D, and E), Supporting Information), indicating that the micelles dissolved, whereas for the CLMs, their hydrodynamic diameter was nearly close to the original size (Figure S4 (curve C), Supporting Information) with no polymer detected upon adding THF. Owing to the instability of the disulfide bond in the reductive environment, the excessive GSH (10 mM) was introduced to evaluate the de-cross-linking of the CLMs. After shaking at 37 °C for 6 h, massive smaller matters were found in Figure S4 (curve F) (, Supporting Information), similar to the NCMs (curve D), implying that most CLMs were de-cross-linked successfully in the reductive medium.

Cytotoxicity and HepG2 Cell Growth Inhibition Assays. Dose-dependent cytotoxicity profiles for the drug-free control cross-linked PEG_{43}-*b*-P(AA_{30}-*co*-tBA_{18})-*b*-PCL_{53} micelles with or without being treated with 10 mM GSH for 48 h, the DOX-loaded cross-linked PEG_{43}-*b*-P(AA_{30}-*co*-tBA_{18})-*b*-PCL_{53} micelles, and free DOX are shown in Figure 3. In the absence of drug, the cross-linked PEG_{43}-*b*-P(AA_{30}-*co*-tBA_{18})-*b*-PCL_{53} micelles were reasonably safe up to 300 μg/mL (cell viability >93.1%) and exhibited a similar biocompatibility after the their disulfide bonds had been de-cross-linked.

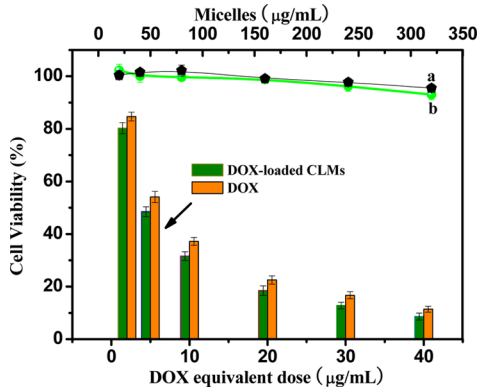

Figure 3. Cell viability assay in HepG2 cell (mean ± standard deviation; $n = 5$). The cells were treated with the cross-linked PEG_{43}-*b*-P(AA_{30}-*co*-tBA_{18})-*b*-PCL_{53} micelles with (b) or without (a) being treated with 10 mM GSH for 48 h, the DOX-loaded cross-linked PEG_{43}-*b*-P(AA_{30}-*co*-tBA_{18})-*b*-PCL_{53} micelles, and the free DOX at 37 °C for 24 h.

The free DOX significantly reduced the viability of the HepG2 cell line. In a dose-dependent manner, the concentration killing 50% of the cells (IC_{50}) is estimated to be smaller than 6.2 μg/mL. The growth inhibition tests showed that the free DOX and the DOX-loaded cross-linked PEG_{43}-*b*-P(AA_{30}-*co*-tBA_{18})-*b*-PCL_{53} micelles exhibited similar anticancer activity. Furthermore, the DOX-loaded cross-linked PEG_{43}-*b*-P(AA_{30}-*co*-tBA_{18})-*b*-PCL_{53} micelles had an estimated IC_{50} smaller than 23.0 μg/mL. These results imply that DOX could be efficiently released from the DOX-loaded cross-linked PEG_{43}-*b*-P(AA_{30}-*co*-tBA_{18})-*b*-PCL_{53} micelles after cell internalization in the reductive microenvironment of the cancer tissues. Considering a DEE of approximately 57% (w/w) (Table 1), the apparent cytotoxicty of the DOX-loaded cross-linked PEG_{43}-*b*-P(AA_{30}-*co*-tBA_{18})-*b*-PCL_{53} micelles was observed, and the anticancer activity was slightly higher than the free DOX, indicating that the cross-linked PEG_{43}-*b*-P(AA_{30}-*co*-tBA_{18})-*b*-PCL_{53} micelles

dx.doi.org/10.1021/am505531e | ACS Appl. Mater. Interfaces 2015, 7, 166−174

not only display remarkable biocompatibility but also possess excellent anticancer activity.

DOX Loading and Controlled Release. As a DDS, it is important to assess DLC and DEE of the cross-linked PEG_{43}-*b*-P(AA_{30}-*co*-*t*BA_{18})-*b*-PCL_{53} micelles (CLMs) and the non-cross-linked PEG_{43}-*b*-P(AA_{30}-*co*-*t*BA_{18})-*b*-PCL_{53} micelles (NLMs). The hydrophobic blocks are expected to encapsulate an effectively large amount of DOX during the self-assembly of the amphiphilic copolymer. To optimize the CMC, DLC, and DEE of the PEG_{43}-*b*-P(AA_n-*co*-*t*BA_{48-n})-*b*-PCL_{53} micelles, control hydrolysis experiments were carried out. The DLC and DEE of the micelles increased with the increase of the hydrophilic moieties (Table 1). This suggests that the increase in DLC is mainly due to the electrostatic interaction between the amine groups of DOX and the carboxylic acid groups of the PAA segments. The DLC and DEE of the CLMs were lower than the NCMs under the same conditions and might be due to the fact that the amidation between cystamine and the PAA segments weakens the electrostatic interaction between DOX and the PAA segments. It could also be revealed by the difference of zeta potentials between CLMs and DOX-loaded CLMs. The zeta potential increased from −32.32 to −22.31 mV after DOX loading. However, the cross-linking of micelles is an undoubtedly accepted approach, owing to the enhanced stability, improving the morphologies and size distribution.

The GSH level and extracellular pH in normal tissues and blood are approximately 10 μM and 7.4, respectively. Importantly, the endosomes and lysosomes have high GSH level (10 mM) and are drastically acidic (pH 4.5−6.5). Furthermore, therapeutically required release of DOX from the cross-linked PEG_{43}-*b*-P(AA_{30}-*co*-*t*BA_{18})-*b*-PCL_{53} micelles is predicted to be accelerated under reductive and acidic conditions in an endosome because the high level of GSH can cut off the disulfide bonds. Considering these differences, the *in vitro* controlled release from the DOX-loaded CLMs was performed at 37 °C under different conditions, i.e., (i) pH 7.4, (ii) pH 7.4 with 10 μM GSH, (iii) pH 5.0 without GSH, and (iv) pH 5.0 with 10 mM GSH. In addition, the release from the DOX-loaded NCMs was performed in PBS at pH 7.4 and 5.0.

The cumulative release from the DOX-loaded NCMs was 25.44% at physiological pH and 10.54% from the DOX-loaded CLMs (Figure 4). In addition, the cumulative release ratio from the NCMs was 52.80% at pH 5.0 and from the CLMs was only 43.26%. The cumulative release of the CLMs was lower than that from the NCMs, resulting from the cross-linking of the shells. The release from both the DOX-loaded CLMs and NCMs increased in weak acidic medium (pH 5.0), attributed to the increase in solubility of DOX resulting in the faster diffusion of DOX (solubility of DOX: 0.51 ± 0.04 mg/mL in pH 7.4 PBS and 1.04 ± 0.05 mg/mL in pH 5.0 PBS). The cumulative release ratio of the CLMs reached 31.32% within 465 min, whereas that from the NCMs reached 31.90% within only 285 min. That is to say, the cross-linking of the PAA shells could efficiently bring down the DOX release.

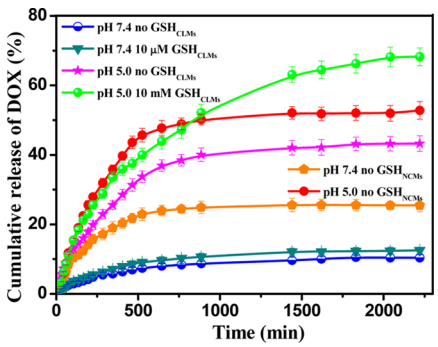

Figure 4. Cumulative DOX release from the DOX-loaded micelles in the simulated bodily fluids (SD < 1%, n = 3).

To simulate the intracellular trafficking process, drug release experiments were conducted at pH 5.0 with 10 mM GSH (mimicking endosome). In comparison with pH 5.0 without GSH, the cumulative release at pH 5.0 with 10 mM GSH was 68.24% (Figure 4). Notably, DOX is effectively released in elevated GSH environments, and the cumulative release from the CLMs apparently increased under acidic conditions with GSH (12.52 wt % at pH 7.4 with 10 μM GSH and 68.24 wt % at pH 5.0 with 10 mM GSH, respectively). This finding demonstrates that the premature release of DOX during blood circulation is minimized because of the better stability of the cross-linked shells at pH 7.4 with 10 μM GSH. The initial release is 5-fold faster at pH 5.0 with 10 mM GSH than at pH 7.4 with 10 μM GSH. The results indicated that the proposed CLMs possessing the ideal structure for DDS could reduce severe side effects because of lower premature DOX concentration during blood circulation.[9]

Then the Higuchi and Korsmeyer-Peppas models were used to fit the accumulative release (Figure S5, Supporting Information), and the correlation coefficients (R^2) were used to evaluate the fitting accuracy. Furthermore, to shed light on the release mechanism, typical conditions of release media were chosen, such as pH 7.4 in the absence of GSH, pH 5.0 in the absence of GSH, and pH 5.0 in the presence of 10 mM GSH at 37 °C, for that of the NCMs at pH 7.4. Linearities with R^2 of 0.9551, 0.9559, 0.9746, and 0.8917 were calculated from the Higuchi plots of the DOX-loaded CLMs and DOX-loaded NCMs, respectively.

As for the Korsmeyer-Peppas model (Figure S5 (b.d.f.h), Supporting Information), the plots for the DOX-loaded CLMs resulted in linearity with R^2 and n values of 0.9795 and 0.5109, 0.9847 and 0.5747, and 0.9467 and 0.6602, and those of the NCMs were 0.9111 and 0.6341, respectively. It also yielded comparatively good linearities and ordered release exponents. The n values were between 0.43 and 0.85, indicating the release mechanism from the DOX-loaded CLMs and NCMs in all conditions were the anomalous transport.[22,29] Compared with the CLMs at pH 7.4, the release exponent from the NCMs was 0.6341, higher than 0.5109, indicating that cross-linked shells hindered efficiently the release of DOX, in comparison with the NCMs. Decreasing pH from 7.4 to 5.0, the release exponent for the CLMs increased from 0.5109 to 0.5747. In the slight acidic conditions, the solubility of DOX increases along with decreasing pH value in the PBS. It accelerates the release, which results in a higher release exponent at pH 5.0. Consequently, the comprehensive process leads to the anomalous transport. But even more crucial, the release exponent (0.6602) in the presence of 10 mM GSH was higher than without GSH. A possible explanation may be that the de-cross-linking of the disulfide bonds unlocks the resistance of the cross-linked shells, which accelerates the release of DOX. These synergetic results suggest that the release mechanism from both the DOX-loaded CLMs and NCMs identified highly with their release behaviors. In conclusion, the release mechanism and behaviors commit the design philosophy of the drug delivery

dx.doi.org/10.1021/am505531e | ACS Appl. Mater. Interfaces 2015, 7, 166−174

vesicles with unique structure and reduction-responsive property.

CLSM Analysis. The CLSM technique was utilized to evaulate cellular uptake of the DOX-loaded CLMs for HepG2 cells (Figure 5). It is worth noting that strong DOX

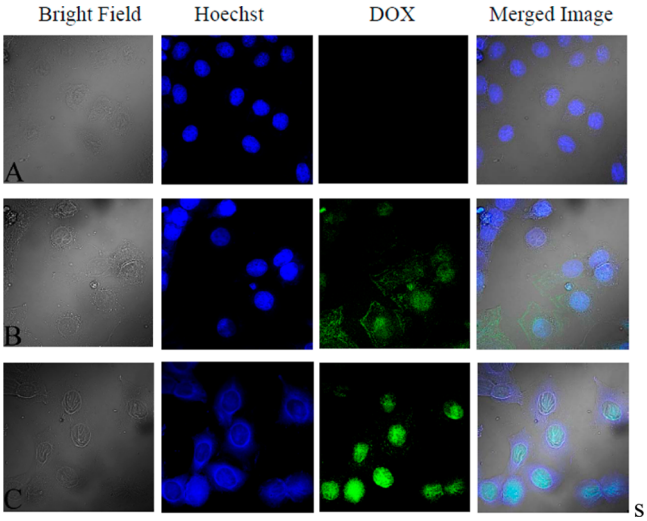

Figure 5. CLSM images of cellular uptake of the free DOX and the DOX-loaded CLMs with HepG2 cells after 6 h incubation. (A) HepG2 cells were stained by Hoechst, (B) free DOX control (30 μg/mL DOX), and (C) DOX-loaded CLMs (30 μg DOX equiv/mL), respectively.

fluorescence appeared for the cells after 6 h incubation with the DOX-loaded CLMs, demonstrating the efficient uptake of the DOX-loaded CLMs and remarkable intracellular release of DOX. But even more crucial, this result shows that the design of disulfide bonds within the core−shell−corona DDS of PEG_{43}-*b*-P(AA_{30}-*co*-*t*BA_{18})-*b*-PCL_{53} micelles is cleaved inside cancer cells in correspondence with the reductive media with high-level GSH (2−10 mM).[30] In addition, the fluorescence images indicated that DOX has been efficiently released from the DOX-loaded cross-linked PEG_{43}-*b*-P(AA_{30}-*co*-*t*BA_{18})-*b*-PCL_{53} micelles to cytosol. Obviously, the CLSM analysis showed that most DOX has also been transported into the nucleus (Figure 5C) within 6 h incubation compared with the free DOX, which was accumulated mainly in the cytoplasm (Figure 5B). The results imply that the DOX-loaded CLMs efficiently carried DOX to the cell nucleus, as reported previously.[31] Notably, the latter stronger fluorescence emerged image indicates that DOX released from the DOX-loaded CLMs was accumulated mainly in the nucleus in comparison with the free DOX (Figure 5B and C).

It should be further noted that the DNA in the cell nucleus was destroyed by intercalation of the released DOX from the DOX-loaded CLMs in 6 h incubation (as shown Figure 5C). Interestingly, the broken moieties of the DNA diffused external microenvironment of HepG2 cells were displayed in the merged image (Figure 5C). Furthermore, it has been reported that DOX can freely diffuse through the endolysosomal membrane and enter the nucleus. Thus, it intercalates into DNAs, leading to the intranuclear accumulation of DOX.[32] This observation is in accordance with the results of the main mechanism of DOX's antitumor activity, which induce single- and double-strand breaks in DNAs and disrupt the replication and transcription processes in cancer cells.[33] In conclusion, the CLSM analysis demonstrates that the DOX-loaded CLMs are internalized successfully for HepG2 cells, and the DOX released from the DOX-loaded CLMs is accumulated mainly in the cell nucleus and might break the single and double strand of the DNAs inside.

CONCLUSIONS

Triblock copolymer (PEG_{43}-*b*-P(AA-*co*-*t*BA)-*b*-PCL_{53}) prepared via combination of ROP, ATRP, click chemistry, and hydrolyzation was cross-linked with the disulfide bond to assemble into stimuli-regulated core−shell−corona micelles in aqueous solution, in order to solve the major obstacle for anticancer delivery—the premature drug release during blood circulation—so the drugs encapsulated can be released more rapidly in the specifically targeted disease sites to enhance the therapeutic efficacy. The micelles of the optimized copolymer, PEG_{43}-*b*-P(AA_{30}-*co*-*t*BA_{18})-*b*-PCL_{53}, had a high DOX-loading capacity (31.1%) as well as high drug encapsulation efficiency (62.2%). They showed slow sustained release in physiological conditions and a rapid release upon exposure to the simulated intracellular reductive conditions, and the release rate and the amount of released drug could be tuned by the cross-linked PAA shells. In addition, the micelles displayed remarkable biocompatibility and excellent anticancer activity similar to the free DOX. The CLSM analysis demonstrated that the DOX-loaded CLMs were internalized successfully for HepG2 cells and accumulated mainly in the cell nucleus. Therefore, the core−shell−corona micelles are expected to be attractive "smart" reduction-responsive nanovehicles for tumor microenvironment-responsive controlled delivery of hydrophobic anticancer drugs.

ASSOCIATED CONTENT

Supporting Information

The FT-IR, GPC, fractionated gain of the signals of ^{1}H NMR results, and dynamic analysis of the drug release. This material is available free of charge via the Internet at http://pubs.acs.org.

AUTHOR INFORMATION

Corresponding Author

*Tel./Fax: 86 0931 8912582. E-mail: pliu@lzu.edu.cn.

Notes

The authors declare no competing financial interest.

ACKNOWLEDGMENTS

This project was granted financial support from the National Nature Science Foundation of China (Grant no. 20904017) and the Program for New Century Excellent Talents in University (Grant no. NCET-09-0441).

REFERENCES

(1) Ge, Z. S.; Liu, S. Y. Functional Block Copolymer Assemblies Responsive to Tumor and Intracellular Microenvironments for Site-specific Drug Delivery and Enhanced Imaging Performance. *Chem. Soc. Rev.* **2013**, *42*, 7289−7325.

(2) Bastakoti, B. P.; Wu, K. C. W.; Inoue, M.; Yusa, S.; Nakashima, K.; Yamauchi, Y. Multifunctional Core-Shell-Corona-Type Polymeric Micelles for Anticancer. *Chem.—Eur. J.* **2013**, *19*, 4812−4817.

(3) Szakacs, G.; Paterson, J. K.; Ludwig, J. A.; Booth-Genthe, C.; Gottesman, M. M. Targeting multidrug resistance in cancer. *Nat. Rev. Drug Discovery* **2006**, *5*, 219−234.

(4) Zhuang, J. M.; Gordon, M. R.; Ventura, J.; Li, L. Y.; Thayumanavan, S. Multi-stimuli responsive macromolecules and their assemblies. *Chem. Soc. Rev.* **2013**, *42*, 7421−7435.
(5) Wang, Y. C.; Li, Y.; Sun, T. M.; Xiong, M. H.; Wu, J.; Yang, Y. Y.; Wang, J. Core−Shell−Corona Micelle Stabilized by Reversible Cross-Linkage for Intracellular Drug Delivery. *Macromol. Rapid Commun.* **2010**, *31*, 1201−1206.
(6) van Nostrum, C. F. Covalently Cross-linked Amphiphilic Block Copolymer Micelles. *Soft Matter* **2011**, *7*, 3246−3259.
(7) Murphy, R. F.; Powers, S.; Cantor, C. R. Endosome pH Measured in Single Cells by Dual Fluorescence Flow Cytometry: Rapid Acidification of Insulin to pH 6. *J. Cell Biol.* **1984**, *98*, 1757−1762.
(8) Go, Y. M.; Jones, D. P. Redox Compartmentalization in Eukaryotic Cells. *Biochim. Biophys. Acta, Gen. Subj.* **2008**, *1780*, 1271−1290.
(9) Yue, J.; Wang, R.; Liu, S.; Wu, S. H.; Xie, Z. G.; Huang, Y. B.; Jing, X. B. Reduction-responsive Shell-crosslinked Micelles Prepared from Y-shaped Amphiphilic Block Copolymers as a Drug Carrier. *Soft Matter* **2012**, *8*, 7426−7435.
(10) Xu, H. F.; Meng, F. H.; Zhong, Z. Y. Reversibly Crosslinked Temperature-responsive Nano-sized Polymersomes: Synthesis and Triggered Drug Release. *J. Mater. Chem.* **2009**, *19*, 4183−4190.
(11) Wei, X. W.; Gong, C. Y.; Gou, M. L.; Fu, S. Z.; Guo, Q. F.; Shi, S.; Luo, F.; Guo, G.; Qiu, L. Y.; Qian, Z. Y. Biodegradable Poly(ε-caprolactone)−poly(ethylene glycol) Copolymers as Drug Delivery System. *Int. J. Pharm.* **2009**, *381*, 1−18.
(12) Yan, J. L.; Ye, Z. Y.; Chen, M.; Liu, Z. Z.; Xiao, Y.; Zhang, Y.; Zhou, Y.; Tan, W. S.; Lang, M. D. Fine Tuning Micellar Core-Forming Block of Poly(ethylene glycol)-block-poly(ε-caprolactone) Amphiphilic Copolymers Based on Chemical Modification for the Solubilization and Delivery of Doxorubicin. *Biomacromolecules* **2011**, *12*, 2562−2572.
(13) Chen, J. C.; Liu, M. Z.; Gong, H. H.; Huang, Y. J.; Chen, C. Synthesis and Self-Assembly of Thermoresponsive PEG-b-PNIPAM-b-PCL ABC Triblock Copolymer through the Combination of Atom Transfer Radical Polymerization, Ring-Opening Polymerization, and Click Chemistry. *J. Phys. Chem. B* **2011**, *115*, 14947−14955.
(14) Lin, D. S.; Jiang, Q.; Cheng, Q.; Huang, Y. Y.; Huang, P. S.; Han, S. C.; Guo, S. T.; Liang, Z. C.; Dong, A. J. Polycation-detachable Nanoparticles Self-assembled from mPEG-PCL-g-SS-PDMAEMA for In Vitro and In Vivo siRNA Delivery. *Acta Biomater.* **2013**, *9*, 7746−7757.
(15) Sun, P. J.; Zhang, Y.; Shi, L. Q.; Gan, Z. H. Thermosensitive Nanoparticles Self-assembled from PCL-b-PEO-b-PNIPAAm Triblock Copolymers and Their Potential for Controlled Drug Release. *Macromol. Biosci.* **2010**, *10*, 621−631.
(16) Endres, T.; Zheng, M. Y.; Kilic, A.; Turowska, A.; Beck-Broichsitter, M.; Renz, H.; Merkel, O. M.; Kissel, T. Amphiphilic Biodegradable PEG-PCL-PEI Triblock Copolymers for FRET-Capable In Vitro and In Vivo Delivery of siRNA and Quantum Dots. *Mol. Pharmaceutics* **2014**, *11*, 1273−1281.
(17) Ren, T. B.; Liu, Q. M.; Lu, H.; Liu, H. M.; Zhang, X.; Du, J. Z. Multifunctional Polymer Vesicles for Ultrasensitive Magnetic Resonance Imaging and Drug Delivery. *J. Mater. Chem.* **2012**, *22*, 12329−12338.
(18) Liu, Q. M.; Chen, J.; Du, J. Z. Asymmetrical Polymer Vesicles with a "Stealthy" Outer Corona and an Endosomal-Escape-Accelerating Inner Corona for Efficient Intracellular Anticancer Drug Delivery. *Biomacromolecules* **2014**, *15*, 3072−3082.
(19) Kricheldorf, H. R.; Kreiser-Saunders, I.; Stricker, A. Polylactones 48. $SnOct_2$-initiated Polymerizations of Lactide: A Mechanistic Study. *Macromolecules* **2000**, *33*, 702−709.
(20) Zeng, J.; Du, P. C.; Liu, P. One-pot Self-assembly Directed Fabrication of Biocompatible Core Cross-linked Polymeric Micelles as a Drug Delivery System. *RSC Adv.* **2013**, *3*, 19492−19500.
(21) Yuan, Y. Y.; Wang, Y. C.; Du, J. Z.; Wang, J. Synthesis of Amphiphilic ABC 3-Miktoarm Star Terpolymer by Combination of Ring Opening Polymerization and "Click" Chemistry. *Macromolecules* **2008**, *41*, 8620−8625.
(22) Higuich, T. Rate of Release of Medicaments from Ointment Bases Containing Drugs in Suspension. *J. Pharm. Sci.* **1961**, *50*, 874−875.
(23) Siepmann, J.; Peppas, N. A. Modeling of Drug Release from Delivery Systems Based on Hydroxypropyl methylcellulose (HPMC). *Adv. Drug Delivery Rev.* **2001**, *48*, 139−157.
(24) Zhao, X. B.; Liu, L.; Li, X. R.; Zeng, J.; Jia, X.; Liu, P. Biocompatible Graphene Oxide Nanoparticle-Based Drug Delivery Platform for Tumor Microenvironment-Responsive Triggered Release of Doxorubicin. *Langmiur* **2014**, *30*, 10419−10429.
(25) Bao, H. Q.; Li, L.; Gan, L. H.; Ping, Y.; Li, J.; Ravi, P. Thermo- and pH-Responsive Association Behavior of Dual Hydrophilic Graft Chitosan Terpolymer Synthesized via ATRP and Click Chemistry. *Macromolecules* **2010**, *43*, 5679−5687.
(26) Que emener, D.; Davis, T. P.; Barner-Kowollik, C.; Stenzel, M. H. Functionalization of Polymers with Phosphorescent Iridium Complexes via Click Chemistry. *Chem. Commun.* **2006**, 5051−5053.
(27) Chambon, P.; Blanazs, A.; Battaglia, G.; Armes, S. P. How Does Cross-Linking Affect the Stability of Block Copolymer Vesicles in the Presence of Surfactant? *Langmuir* **2012**, *28*, 1196−1205.
(28) Yue, J.; Wang, R.; Liu, S.; Wu, S. H.; Xie, Z. G.; Huang, Y. B.; Jing, X. B. Reduction-responsive Shell-crosslinked Micelles Prepared from Y-shaped Amphiphilic Block Copolymers as a Drug Carrier. *Soft Matter* **2012**, *8*, 7426−7435.
(29) Raval, A.; Parikh, J.; Engineer, C. Mechanism and In Vitro Release Kinetic Study of Sirolimus from a Biodegradable Polymeric Matrix Coated Cardiovascular Stent. *Ind. Eng. Chem. Res.* **2011**, *50*, 9539−9549.
(30) Sun, H. L.; Guo, B. N.; Li, X. Q.; Cheng, R.; Meng, F. H.; Liu, H. Y.; Zhong, Z. Y. Shell-sheddable Micelles Based on Dextran-SS-poly(e-caprolactone) Diblock Copolymer for Efficient Intracellular Release of Doxorubicin. *Biomacromolecules* **2010**, *11*, 848−854.
(31) Xue, X. D.; Zhao, Y. Y.; Dai, L. R.; Zhang, X.; Hao, X. H.; Zhang, C. Q.; Huo, S. D.; Liu, J.; Liu, C.; Kumar, A.; Chen, W. Q.; Zou, G. Z.; Liang, X. J. Spatiotemporal Drug Release Visualized through a Drug Delivery System with Tunable Aggregation-Induced Emission. *Adv. Mater.* **2014**, *26*, 712−717.
(32) Lale, S. V.; Aswathy, R. G.; Aravind, A.; Kumar, D. S.; Koul, V. AS1411 Aptamer and Folic Acid Functionalized pH-Responsive ATRP Fabricated pPEGMA−PCL−pPEGMA Polymeric Nanoparticles for Targeted Drug Delivery in Cancer Therapy. *Biomacromolecules* **2014**, *15*, 1737−1752.
(33) Tewey, K. M.; Rowe, T. C.; Yang, L.; Halligan, B. D.; Liu, L. F. Adriamycin-induced DNA Damage Mediated by Mammalian DNA Topoisomerase II. *Science* **1984**, *226* (4673), 466−468.